Adaptive Coding and Modulation for Robust Optical Access Networks

Elaine S. Chou and Joseph M. Kahn, *Fellow, IEEE*

***Abstract*—We introduce adaptive coding and modulation (ACM) to direct-detection passive optical networks (PONs) operating beyond 10 Gb/s per wavelength to allow each user to transmit at the highest possible bit rate and improve network reliability. Current fixed-rate PONs must allocate significant power margin to ensure reliable long-term operation over channels that vary over time and between users. Introducing adaptive-rate transceivers with ACM is a promising low-cost solution to increasing the overall capacity of optical access networks. The proposed ACM scheme uses two-, three-, or four-level pulse-amplitude modulation (2-, 3-, or 4-PAM) at a fixed symbol rate with direct detection and low-density parity check (LDPC) codes derived from a mother code by shortening and puncturing, decoded using fixed-initialization normalized min-sum decoding. The scheme supports received optical powers spanning a 10-dB range at bit rates of 20–54 Gb/s. In a PON with 64 users transmitting at a symbol rate of 30 Gbaud and a maximum transmission distance of 25 km, the ACM scheme demonstrates more than 3 dB improvement in overall optical power budget. For a fixed margin, ACM can increase throughput up to 60% compared to fixed-rate transmission, from 25 Gb/s to 39.7 Gb/s, or from 37.5 Gb/s to over 50 Gb/s, depending on the received optical power.**

***Index Terms*—Adaptive coding and modulation, direct detection, information rates, optical fiber communication, time division multiaccess.**

I. Introduction

INTERNET traffic growth has brought optical fiber ever closer to the end user. Fiber is the dominant access medium in Korea, Japan, and several countries in Europe, and its share throughout the world is growing [1]. Although access network optical links have much lower bit rates than their data center or long-haul counterparts, the asymmetric, point-to-many structure of access networks that have one optical line terminal (OLT) in communication with many optical networking units (ONUs) leads to many challenges unique to access. Cost and reliability considerations constrain fiber access networks to use passive optical distribution networks, direct detection, and inexpensive components. Innovative architectures can scale out passive optical networks (PONs) to support many users over a long reach (e.g., 768 users over 50 km at 2.5 Gb/s [2]). However, scaling to bit rates above 10 Gb/s is difficult, because of optical power budget constraints and distortion from fiber chromatic dispersion (CD) and bandwidth limitations in optoelectronic and electronic components.

Supporting higher bit rates in PONs will likely require improving power budgets by using advanced optoelectronic components, such as state-of-the art avalanche photodiodes (APDs) [3]. However, more advanced modulation and coding techniques can also help support higher bit rates. Introducing adaptive coding and modulation (ACM) into PONs can enable each user to transmit and receive at the highest bit rate their link can support reliably. When using ACM, most link degradations caused by component aging or variations, optical connector problems, or unexpected noise or interference, will cause graceful degradation to a lower bit rate instead of a complete loss of connection, allowing time for corrective action if needed. In many situations, the user may not notice any impact. While PONs are traditionally designed with several dB of optical power loss margin to ensure reliable long-term operation, it will be increasingly difficult and costly to follow this approach as PONs scale beyond 10 Gb/s. Flexible PONs using ACM to complement physical improvements, such as efficient optical distribution network (ODN) designs and low-noise APDs, can be deployed with lower margin, enabling scaling to more users and higher bit rates.

Most other communication systems, as technology matures, have made the transition to ACM. For example, wireless systems, with channels subject to large time-varying channel fluctuations, widely use ACM [4]. The high-level benefit of variable-rate transceivers in long-haul optical systems is investigated in [5], and ACM in other types of optical communication channels have been studied [6]. A theoretical study of coded phase-shift keying for a coherent system with different detection schemes was performed in [7]. Deployed long-haul optical fiber systems now use ACM, and may perform optimization of modulation, coding and launched power among many wavelength-division multiplexed (WDM) channels [8]. Most previous studies of rate adaptation in PONs focus on decreasing energy consumption [9], [10]. The possibility of using multiple modulation formats with fixed forward error correction (FEC) for higher throughput in PONs has been explored [11], [12]. Other rate adaptation methods in PONs, such as adaptive bit loading with OFDM [10], [13] or use of variable symbol rates [14], have been studied as well. This paper investigates the benefits of an adaptive coding and modulation scheme that can be applied to existing PON

Manuscript received August 10, 2019; revised October 14, 2019 and December 11, 2019; accepted December 23, 2019. Date of publication December 31, 2019; date of current version April 15, 2020. This work was supported by a Rambus Corporation Stanford Graduate Fellowship. *(Corresponding author: Elaine S. Chou.)*

The authors are with E. L. Ginzton Laboratory, Department of Electrical Engineering, Stanford University, Stanford, CA 94305 USA (e-mail: eschou@stanford.edu; jmk@ee.stanford.edu).

Color versions of one or more of the figures in this article are available online at http://ieeexplore.ieee.org.

Digital Object Identifier 10.1109/JLT.2019.2963276

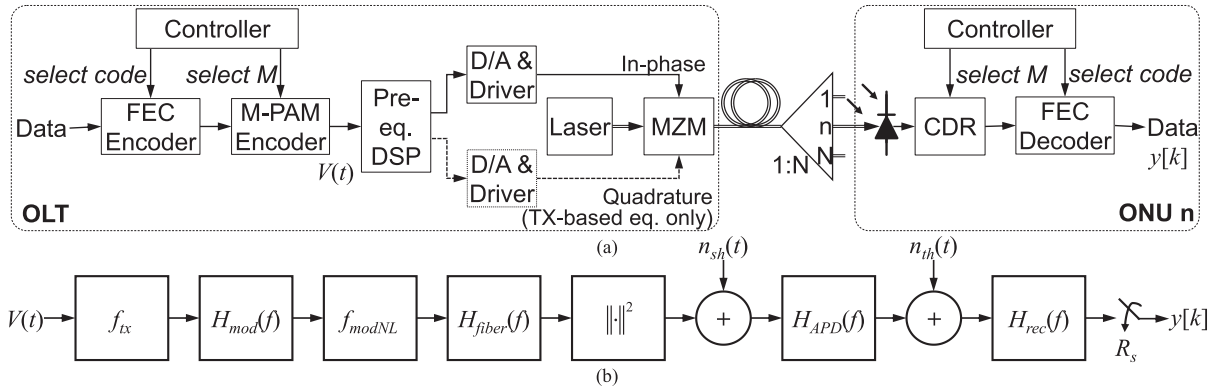

Fig. 1. Block diagram of PON with ACM showing (a) functional blocks and (b) mathematical model of the optical channel from the electrical waveform $V(t)$ at the output of the M-PAM mapper to the final decoded symbols $y[k]$. Dashed blocks denote optional blocks for transmitter-based equalization. In (b), $H_{\mathrm{mod}}(f)$, $H_{fiber}(f)$, and $H_{APD}(f)$ are the frequency response of the DAC and MZM, fiber CD, and APD respectively. f_{tx} is the transmitter-based pre-equalization function that applies interleaved instantaneous nonlinear operations and frequency domain transformations, and if no pre-equalization is applied it simply adjusts the PAM levels to invert the MZM nonlinearity. $f_{\mathrm{mod}\,NL}$ is the instantaneous nonlinearity applied by the modulator. $H_{rec}(f)$ is the frequency response of the antialiasing filter.

architectures with minimal changes, expanding on the ACM scheme proposed in [15]. The system employs variable-order multilevel pulse amplitude modulation (PAM) and variable-rate FEC codes, a combination attractive for its high performance and low complexity. It requires only one wavelength but is also compatible with wavelength-division-multiplexed systems. Our system has a fixed symbol rate and employs three modulation formats; 2-, 3-, and 4-PAM; as well as variable FEC overhead that is adjusted via puncturing and shortening of a low-density parity-check (LCPC) code. As analog-to-digital converters (ADCs) are typically not used in PONs, in place of log-likelihood soft inputs, the LDPC decoder uses fixed initialization for compatibility with soft-decoding algorithms [16], [17]. In addition to demonstrating the advantages of this ACM system, we compare different equalization techniques and study tradeoffs between the number of rate steps and the benefits obtained.

The remainder of this paper is organized as follows. In Section II, we describe the transmission system design including the system model used in analysis. In Section III, we detail the mechanism for rate adaptation with ACM. In Section IV, we present a probabilistic model for the optical power loss of ONUs in a PON and highlight the benefits yielded by ACM as determined through simulation.

II. Transmission System

A general block diagram for the downlink in a rate-adaptive PON using ACM is shown in Fig. 1a. The scheme shown has controllers at the transmitter and receiver that regulate the FEC rate and PAM modulation order to employ ACM. Fig. 2 shows an example intensity waveform received in three consecutive user time slots. Because of different link conditions, these three users are receiving information at low, intermediate, and high rates. The M-PAM signal is modulated with a Mach-Zehnder modulator (MZM) and detected using an APD. Equalization can be applied to decrease the effect of CD and bandwidth limitations, and further improve the power budget, at higher

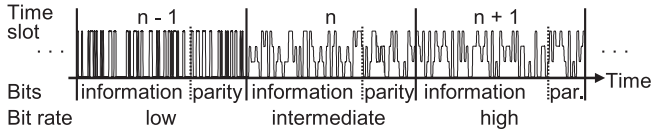

Fig. 2. Intensity waveforms during three consecutive user time slots using variable-rate codes with 2-PAM, 3-PAM, and 4-PAM to achieve low, intermediate, and high bit rates.

deployment cost. To analyze the effect of system parameters, we develop a baseband model for the channel starting at the output of the M-PAM symbol mapper and ending at the decoded symbol, shown in Fig. 1b.

A. Transmitter

At the transmitter, a stream of input bits is encoded using a binary linear block code. Then, the coded bits are mapped to M-PAM intensity levels. Some methods such as dual-rate time-division multiple access (TDMA) in 10G Ethernet PON (EPON) [18] vary the symbol rate to support more than one rate, but to facilitate synchronization, we keep the symbol rate the same for all users on a given downlink. A direct-detection system is restricted to a signal constellation on the positive real axis of the in-phase and quadrature plane, so we use unipolar PAM of orders 2, 3, and 4, corresponding to 1, 1.5, and 2 bits per symbol, respectively. 2-PAM is equivalent to on-off keying (OOK). 2-PAM and 4-PAM use the basic linear M-PAM signal constellation of Fig. 3b with $M = 2$ and $M = 4$ respectively. For these constellations, Gray coding can be used to ensure that adjacent points differ by only one bit flip, so for low symbol-error probability p_e, the bit-error ratio (BER) is $p_b \approx 2(M-1)/(M \log M) \cdot p_e$. Bit errors are independent, so we can construct an analogous binary symmetric channel (BSC) with transition probability p_b to evaluate FEC performance with a nonbinary PAM constellation.

For 3-PAM, we use the two-dimensional (2D) signal constellation shown in Fig. 3a. The two dimensions correspond to consecutive symbol intervals, with three signal levels in each

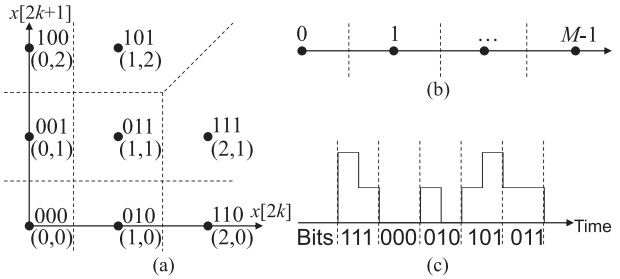

Fig. 3. Signal constellations with dashed decision boundaries: (a) probabilistically-shaped 2-dimensional (PS 2D) 3-PAM with bit labels and symbol coordinates (b) linear *M*-PAM (c) example PS 2D 3-PAM waveform.

dimension and a total of nine possible points. To minimize the average energy per symbol, simple probabilistic shaping (PS) is applied, and the (2, 2) point is eliminated from the signal constellation, leaving 8 points that encode 3 bits per 2D constellation point [19]. A sample waveform is shown in Fig. 3c. The rate of this modulation format is 3 bits/2 symbols = 1.5 bits/symbol. With this signal constellation, Gray coding is not possible because there are three bits per signal point, but the center point has four nearest neighbors, so the constellation points are labelled to minimize the BER given a fixed symbol-error probability. At high signal-to-noise ratio (SNR) near the required BER of the system, errors between the minimum-distance signal points dominate, and the relationship between symbol-error probability and BER is approximately $P_b \approx P_e$. The PS 2D 3-PAM described above can also be interpreted as a primitive code $C \in \{0, 1, 2\}^2 \backslash (2, 2)$ with rate $R_c = \log 8 / \log 9 = 0.95$ that can detect an error if (2,2) is decoded at the channel output. The PS 2D 3-PAM constellation has a 0.3 dB optical power gain compared to linear 3-PAM, as shown in Section IIC.

The system may use OLT-based pre-equalization to mitigate distortion, which is attractive for minimizing ONU complexity. By cascading instantaneous nonlinearities and linear distortions, as well as clipping operations to keep the signal within the proper domain, the transmitter-based pre-equalization function f_{tx} applies an approximate inverse to the channel onto the transmitted signal. Starting with the ideal sampled rectangular intensity waveform, first preemphasis compensates for the limited APD bandwidth by applying the inverse APD frequency response, $H_{APD}^{-1}(f)$. Next, the signal is clipped to retain nonnegativity, and a square-root operation reverses the APD direct detection. Dispersion compensation is applied in the frequency domain with $H_{fiber}^{-1}(f)$. After the signal is clipped to the output range of the MZM, the modulator nonlinearity f_{modNL} is reversed, and preemphasis to counteract bandwidth limitations of the modulator is applied as a frequency domain filter$H_{MZM}^{-1}(f)$. The complete pre-equalization function is

$$f_{tx}\left(X(f)\right) = H_{MZM}^{-1}(f) F\left\{ f_{\mathrm{mod}\ NL}^{-1}\left(F^{-1}\{ H_{APD}^{-1}(f) X(f) \}_{+}^{1/2} \right) \right\}, \quad (1)$$

where $X(f)$ is the frequency domain signal, F and F^{-1} denote Fourier transform and inverse Fourier transform, respectively, and $(\cdot)_+$ denotes taking the nonnegative component.

In performing transmitter-based equalization, the nonnegativity constraint of direct detection, limited output range of the MZM, and limited digital-to-analog converter (DAC) sampling rate prevent a perfect channel inverse transformation. Transmitter-based equalization also increases the peak-to-average power ratio and the signal bandwidth. CD compensation is dependent on transmission distance, so there will be some performance penalty if a common pre-compensation across all ONUs is desired. Two options are to compensate CD for either the longest or average fiber distance. Because the longest link incurs the most fiber attenuation, we choose to compensate for the longest link. CD has a complex-valued transfer function, so for increased compensation capability two MZMs modulate both the in-phase and quadrature components of the transmitted signal. A pre-equalization filter with real taps can be substituted if a single MZM is desired [20]. When pre-equalization is not employed, to relax constraints on the DAC, we use a rectangular pulse shape and adjust the transmitted levels of the *M*-PAM symbols to achieve the desired PAM level spacing after MZM nonlinearity and direct detection.

The pre-equalized signal is low-pass filtered by a DAC. To avoid the chirp induced by directly modulating a laser, we elect to use a MZM to externally modulate the optical signal, which further low-pass filters the signal, then adds a nonlinearity with sinusoidal transfer characteristic. The low-pass filtering of the DAC and MZM are combined into $H_{mod}(f)$.

B. Receiver

After the modulated signal is distributed to all ONUs through the 1:N passive optical splitter, propagating through a single mode fiber (SMF) and undergoing CD described by $H_{fiber}(f)$, it is detected with an APD that uses square-law detection to convert optical power into electrical current. Impact ionization creates a random number of secondary carriers for each absorbed photon, providing gain at the expense of increasing the fluctuations due to shot noise. When the received optical power is high enough to ignore the effect of discrete photon arrivals, shot noise can be approximated as a white Gaussian noise with one-sided power spectral density (PSD)

$$S_s = 2qG^2 F_A\left(G\right)\left(RP_{rec} + I_d\right), \quad (2)$$

where q is the charge of an electron, G is the APD gain, R is the APD responsivity, P_{rec} the instantaneous received optical power, I_d is the APD dark current, and F_A is the APD excess noise factor given by $F_A(G) = k_A G + (1 - k_A)(2 - 1/G)$, where k_A is the impact ionization factor [21]. The generation of secondary carriers filters the signal with an exponential decay impulse response corresponding to a frequency response $H_{APD}(f)$, limiting the APD bandwidth, and the transimpedance amplifier following the APD adds thermal noise, which is modeled as a white Gaussian noise with one-sided PSD N_0. The Gaussian approximation becomes inaccurate when the APD is in the avalanche buildup time-limited regime, but

for a coded system operating at high BER, the APD gains are low enough to avoid avalanche buildup. When the APD gain is optimized for receiver sensitivity, shot noise and thermal noise are roughly balanced so neither dominates over the other and both must be accounted for.

After conversion into the electrical domain, an analog LPF with frequency response $H_{rec}(f)$ limits the thermal noise bandwidth. During clock and data recovery (CDR), hard decisions are performed on the received symbols, and the signal is mapped back to bits. Finally, the FEC decoder, using initialized values dependent on the demodulated bits as input, corrects errors introduced during transmission to recover the original bits.

C. Optimizing PAM Levels and APD Gain

We consider signal designs that can improve multilevel PAM performance at low cost. A common solution to keeping the same PR30 power budget [18], while increasing rates from 10 Gb/s to 25 or 50 Gb/s, is to use APDs for improved receiver sensitivity compared to PIN photodetectors. However, this improvement comes at a cost of increasing the variance of the signal-dependent shot noise quantified by (2). Optimizing the level spacing to account for signal-dependent noise from APDs has been shown to improve optical power efficiency by over 2 dB in data center links [22].

When the noise variance is dependent on the signal level, the optimal decision moves towards the levels with smaller noise variances [21]. For more than two levels, adjusting the spacing between levels to distribute errors across all decision boundaries can also improve receiver sensitivity. Following the level optimization procedure outlined in [22], we set the *M*-PAM levels to equalize the probability of an incorrect decision at each decision boundary.

The APD gain that optimizes receiver sensitivity for OOK is $G_{opt} = {k_A}^{-1/2}(\sigma_T/qQB + k_A - 1)^{1/2}$ [21], where Q is the Q factor corresponding to the target BER and B is the noise bandwidth. As seen by the Q dependence, the optimal gain is dependent on the target BER, so each code has a unique optimum gain, which differs by approximately 1 dB between the lowest and highest rate codes. However, APD receiver sensitivity is relatively constant near the optimal gain, and fixing the APD gain to optimize the receiver sensitivity using the mother code adds an optical power penalty of less than 0.03 dB for other code rates. The tolerance of receiver sensitivity to slight deviations from the optimal APD gain also extends to higher-order modulation formats. This enables the use of one APD gain for each modulation format across all code rates.

Because hard decisions are made on received symbols, given the transmitted symbol, the optical channel can be described as a discrete memoryless BSC with corresponding transition probabilities. Using optimized level spacing and APD gain, we calculate the mutual information between the transmitted symbols and the received signal under uniform input probability after hard decisions to determine the maximum transmission rate of each modulation format [7], shown in Fig. 4. Optimized level spacing has the potential to improve receiver sensitivity by 1.5 to 2 dB. PS 2D 3-PAM has an optical power shaping gain of 0.5 dB compared to linear 3-PAM. With code rates in the range of 0.67 to 0.92, a rate-adaptation procedure can support a 10-dB range of received optical powers. The curves are about 3 dB away from the soft-decision capacity limit, estimated using the numerical optimization algorithm presented in [23] with an additional average optical power constraint in the maximization.

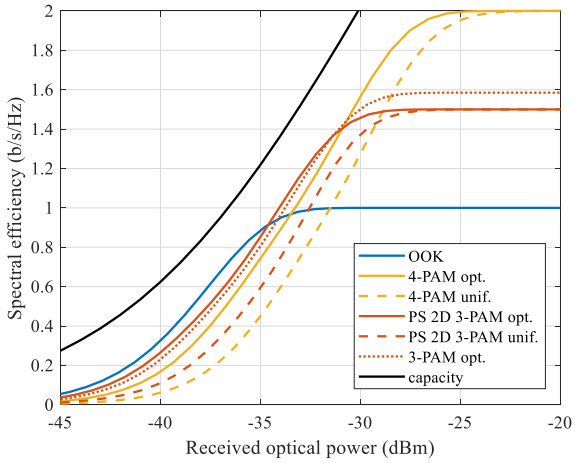

Fig. 4. Comparison of spectral efficiency for OOK, linear 3-PAM, PS 2D 3-PAM, and 4-PAM with uniform and optimized level spacing for a shot and thermal noise-limited direct-detection channel with 12.5 GHz noise bandwidth.

III. Rate Adaptation

The PON ACM method provides discrete rate steps by pairing three *M*-PAM modulation formats with several FEC code rates. Among coding methods, LDPC codes are a practical choice. Without ADCs, only hard symbol decisions are available to the decoder. A family of codes with a range of rates can be created by starting with a mother code in the middle of the range and puncturing or shortening to increase or decrease the rate [24].

A. Forward Error Correction

Linear block codes are used for FEC in many communication systems. They add redundancy to the transmitted bits in exchange for coding gain. PONs have progressed from an optional Reed-Solomon code RS(255,239) in 1G EPON [25] to required RS(255,223) in 10G EPON [18]. For 25G EPON, a single LDPC code is used for higher coding gain compared to Reed-Solomon codes [26]. We select a quasi-cyclic (QC) LDPC code with circulant block size 256, codeword length $n_0 = 16896$ bits, $k_0 = 14336$ information bits, and a rate of $r_0 = 0.85$. One motivation for using QC-LDPC codes is that they are encodable in linear time, in contrast to completely random LDPC codes that can take quadratic time to encode.

LDPC soft-decoding algorithms such as the sum-product and min-sum algorithms typically require soft information from the channel, but fixed-initialization decoding has been proposed to decode LDPC codes using the sum-product algorithm over a BSC [17]. Fixed-initialization decoding enables the use of soft-decoding algorithms with increased error correction capabilities over their hard-decoding counterparts, even when soft

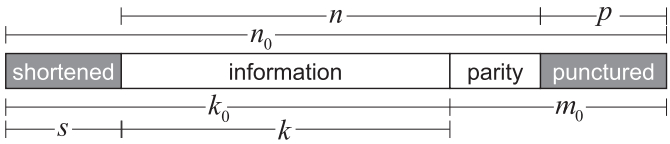

Fig. 5. Shortening deletes s of k_0 information bits, and puncturing deletes p of m_0 parity bits, resulting in a code of rate $r_0 = k/n = (k_0 - s)/(n_0 - p - s)$.

information on the received symbols is not available, as in this PON system with no receiver-side ADCs. To limit decoder complexity, we use the normalized min-sum algorithm [27], a simplified belief propagation decoder algorithm. Because the min-sum algorithm is invariant to initial LLR scaling, the LLR magnitudes can be initialized to 1 for any BSC crossover probability. Then, the log-likelihood ratios (LLRs) of the LDPC decoder are initialized based on the received bits following

$$L_{b_i} = \begin{cases} 1, & b_i = 0 \\ -1, & b_i = 1 \end{cases}, \tag{3}$$

where b_i is the ith codeword bit. The LDPC code has a coding gap of 1.3 dB in SNR and can correct a pre-FEC BER of 8×10^{-3} to a post-FEC BER of 10^{-12} using fixed-initialization normalized min-sum decoding. Although the performance of a binary soft-decision decoder such as the min-sum LDPC decoder is typically most accurately represented by generalized mutual information (GMI) [28], avoiding ADCs and using hard bit decisions discards available soft information. Thus, the channel, as seen by the encoder and decoder pair, is reduced to a BSC with crossover probability equal to the pre-FEC BER. Consequently, pre-FEC BER, typically used to evaluate binary hard-decision codes, is a sufficient metric.

Unlike Reed-Solomon codes, which are based on polynomials over a finite field and have a relatively constrained structure, LDPC codes have numerous degrees of freedom and require careful design. In optical communications, where the post-FEC BER must be extremely low, it is imperative that a code does not exhibit an error floor [29], [30]. There are many methods to design LDPC codes for rate variation, including edge growth and parity splitting [31]; shortening, puncturing, or extending [32]–[35]. We choose to implement rate variation through puncturing and shortening of one LDPC mother code, as shown in Fig. 5, because it enables rate variation of the FEC code with minimal changes in decoding hardware. In shortening, the shortened information bits are fixed to 0 and not transmitted, so they have infinite log-likelihood ratio. This is equivalent to deleting columns of the parity check matrix, so the hardware corresponding to the deleted columns can be disabled. In puncturing, the punctured, untransmitted parity bits are unknown and start at 0 log-likelihood ratio in the iterative decoding algorithm, and the decoding computation remains unchanged. Therefore, shortening and puncturing can be implemented in hardware by a controller that initializes LLR values based on which bits are punctured or shortened at each code rate, eliminating the need for separate decoder hardware for different code rates [36]. Power savings can be achieved by additional control logic that disables

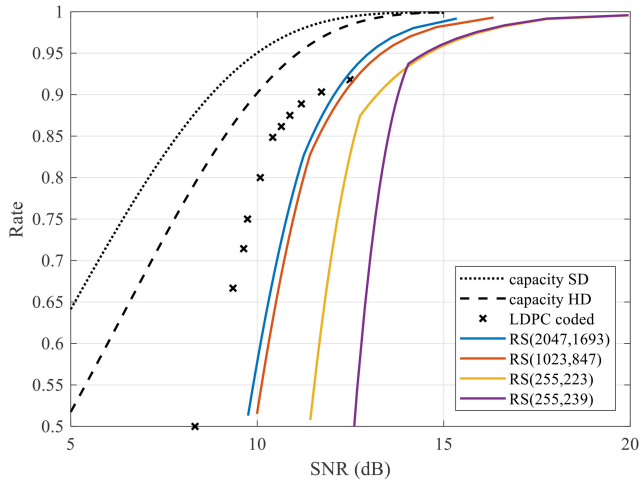

Fig. 6. Code performance comparison on a binary intensity-modulated AWGN channel, comparing simulated LDPC code performance under shortening and puncturing, hard-decision (BSC) and soft-decision (BAWGN) capacity limits, and Reed-Solomon codes of various block lengths.

the redundant hardware components decoding shortened bits already known to be 0. With puncturing and shortening, the new code rate is

$$r = (k_0 - s)/(n_0 - p - s). \tag{4}$$

We implement the fixed-initialization LDPC decoder on an nVidia Tesla K40 GPU for different shortening and puncturing values, using a parallel QC-LDPC min-sum algorithm [37] to decode to a BER below 10^{-12}. By shortening the mother code down to a code rate of ½, or puncturing up to a code rate of 0.92, the required pre-FEC BER ranges from 3.2×10^{-2} to 1.45×10^{-3}. The LDPC code performance is compared against the hard-decision limit and several Reed-Solomon codes in Fig. 6. For a binary code on an additive white Gaussian noise (AWGN) channel, the hard-decision capacity is the capacity of a BSC with crossover probability p, $C = 1 - H(p)$, where $H(p)$ is the binary entropy function. Crossover probability on a binary AWGN channel can be determined by

$$p = Q\left(\frac{d}{2\sigma_n}\right) = Q\left(\sqrt{\frac{\mathrm{SNR}}{2}}\right) \tag{5}$$

for intensity modulated OOK, where d is the distance between the 0 and 1 constellation points in the electrical domain, σ_n is the noise variance, SNR is the electrical SNR, and $Q(\,)$ is the Q function that computes the tail probability of a standard normal distribution.

The performance of Reed-Solomon codes can be estimated analytically for all shortening and puncturing values, while discrete points were simulated for the LDPC code. Generally, as a code is punctured or shortened significantly away from their original code rate, the code's gap to capacity increases, as is observed here. Many algorithms for deciding the order of bits to be deleted in puncturing or shortening to mitigate performance loss have been proposed and studied [33], [35], [38]. For the

simulated LDPC code, the mother code exhibits a performance 1.3 dB away from the hard-decision capacity, while shortening to a rate of ⅔ and puncturing to a rate of 0.92 increase the gap to capacity to 2.6 dB and 2.2 dB, respectively. Lowering the code rate down to ½ introduces significant performance penalty. The LDPC code shows an SNR gain of approximately 1 dB over a slightly longer Reed-Solomon code, but there is a crossover in performance at rates punctured above 0.92. If receiver-based post-equalization is employed and ADCs are added at the receiver, soft information becomes available to the FEC decoder, potentially providing up to 2 dB further improvement in SNR [39].

B. Negotiating Rates

A transmission mode specifies a modulation order and FEC code rate. Each modulation order has a corresponding APD gain and level spacing that optimizes receiver sensitivity. Not all FEC code rates may be paired with every modulation order. In a PON using ACM, an OLT-based controller will set downlink and uplink rates. To accomplish this task, in the PON communication protocol, additional metadata bits are needed to establish the transmission mode used for each ONU. We present one possible method of negotiating rates in the PON. In the downstream direction, the OLT designates the communication mode that following transmissions will use. In the upstream direction, receiving terminals send information about reception quality, either via error-correction decoder input error rate (pre-FEC BER) or a received SNR estimate, to aid the OLT's rate decision [24].

All communication between the OLT and an ONU starts at the lowest rate. The procedure for negotiating rates is as follows: an OLT sends out the call for ONU registrations at the lowest rate, and new ONUs respond with a register request that includes the channel quality information. Based on the channel quality, the OLT can increase the assigned rate of each ONU incrementally until further increases are estimated to be unsupported by current channel conditions. For example, in the case of using pre-FEC BER as the channel quality measure, each FEC rate has a required pre-FEC BER to achieve a post-FEC BER of 10^{-12}, so the OLT can use the pre-FEC BER information to determine which code rates are supported in the channel and possibly increase the rate by more than one rate step at a time. Allowing different code rates to different ONUs from the OLT extracts the most benefit from a variable-rate PON architecture. Current PON protocols support backward compatibility of 1G ONUs in a 10G network by transmitting different rates at different wavelengths. However, to support multiple rates without adding many downstream wavelengths, we elect to use a single wavelength, which will require modifications to the PON MAC frame structure. Synchronization methods must also be designed operate over the wide SNR range supported by ACM.

IV. Network Simulations

To quantify the benefits of introducing rate adaptation into PONs, we perform simulations over the optical link and combine the results with a model for loss distribution. We demonstrate that transmitter-based equalization has performance comparable to receiver-based equalization, without requiring receiver-side ADCs.

TABLE I
Simulation Parameters

Symbol	Quantity	Value	Units
R_s	symbol rate	30	Gbaud
λ	wavelength	1358	nm
λ_0	zero-dispersion wavelength	1310	nm
S_0	dispersion slope	0.092	ps/nm^2·km
D	fiber chromatic dispersion	4.19	ps/nm·km
α	fiber attenuation	0.4	dB/km
L	fiber length	25	km
k_A	APD ionization ratio	0.15	—
R	APD responsivity	0.7	A/W
B_{APD}	APD low-gain bandwidth	22	GHz
I_d	dark current	10	nA
N_0	one-sided thermal noise PSD	9×10^{-22}	A^2/Hz
B_{DAC}	DAC bandwidth	21	GHz
B_{ADC}	ADC bandwidth	15	GHz
$ENOB$	DAC/ADC effective number of bits	5	bits
N_{eq}	number of equalizer taps	15	—

A. Optical Channel Simulation

In simulating the optical network, the symbol rate is chosen such that with a 64b/66b line code and FEC overhead from the mother code, the overall bit rate with OOK is 25 Gb/s, corresponding to a symbol rate of $R_s = 30$ Gbaud. The laser wavelength is set to 1358 nm, corresponding to a downlink in the O band with less dispersion than the C band that leaves some bandwidth closer to the zero-dispersion wavelength for higher-rate protocols as decided for 25G EPON [26], at a cost of increased fiber attenuation. We transmit through 25 km of fiber. Transmitter-based equalization uses a 5-bit DAC with an oversampling rate of 2 to compensate modulator and APD bandwidth limitations, CD, and nonlinearity from the MZM and direct detection. The DAC is modeled as a 5$^{\text{th}}$ order Bessel filter with bandwidth 0.7 times the sampling rate. The MZM is modeled as a critically damped second-order low-pass filter (LPF) followed by a sinusoidal nonlinear transfer function. If no receiver-based equalization is performed, the receiver filtering is an analog 5$^{\text{th}}$ order Bessel filter with cutoff frequency at 0.8 times the symbol rate. If receiver-based equalization is performed, an antialiasing Butterworth filter with cutoff frequency at half the symbol rate is used instead, followed by a 5-bit ADC and an adaptive digital feedforward equalizer. Then, $H_{rec}(f)$ becomes the combined frequency response of the ADC and a continuous-time equivalent of the discrete-time FIR equalization filter. Simulation parameters are summarized in Table I.

Simulation results for the three equalization options after a transmission distance of 25 km are shown in Fig. 7. As PON bit rates scale beyond 10 Gb/s, fiber CD and bandwidth limitations of transmitter and receiver optoelectronic components cause significant distortion and intersymbol interference (ISI) that degrades performance, so we investigate the performance gain

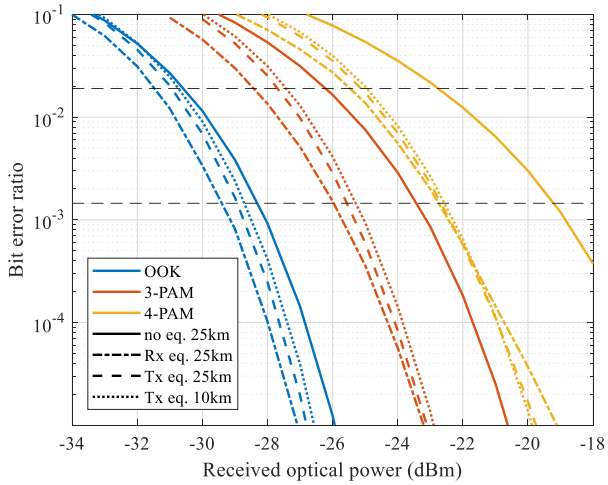

Fig. 7. Simulated performance for the three modulation formats comparing equalization techniques optimized for 25 km transmission distance. Transmission performance with 25 km of fiber is evaluated for the cases of no equalization, receiver-based post-equalization, and transmitter-based pre-equalization. Transmission performance for 10 km of fiber with transmitter-based pre-equalization is also included to demonstrate the small distance-mismatch penalty of common pre-equalization. Horizontal black dashed lines indicate the range of BERs where our family of LDPC codes operates.

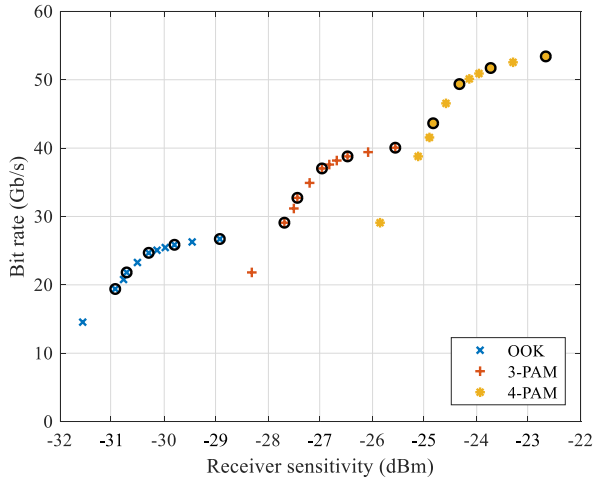

Fig. 8. Simulated performance for all combinations of modulation order and code rate with pre-equalization at 25 km transmission distance. Circled points are selected as transmission modes in throughput increase analysis.

provided by digital equalization. We compare three equalization scenarios: no equalization, transmitter-based pre-equalization, and receiver-based post-equalization. Transmitter-based pre-equalization at 25 km transmission distance eliminates the performance penalty caused by CD, with performance equal to back-to-back transmission. Although direct detection introduces nonlinearity into the channel, a linear filter performing receiver-based post-equalization is still able to provide good signal recovery. An adaptive feedforward filter with 15 symbol-spaced taps converges quickly using gradient descent. Because the LDPC codes used are quite strong and can tolerate a relatively high pre-FEC BER, we do not use decision-feedback equalizers, which may suffer from error propagation at higher BERs.

The penalty of forgoing equalization increases dramatically as the modulation order is increased, because higher-order modulation is more sensitive to distortion. The penalty for distance mismatch in a common transmitter-based equalization scheme that is the same across all ONUs is small, a few tenths of a dB of optical power for 10 km transmission distance with 25 km of CD compensation, much smaller than the 6-dB difference in received optical power due to fiber attenuation. In the target BER range of 10^{-3} to 10^{-2}, our specific implementation of receiver-based post-equalization offers slightly better performance than transmitter-based pre-equalization, with the difference decreasing for lower BER. Due to the asymmetric structure of PONs, transmitter-based equalization is preferred over receiver-based equalization, because of the higher cost of adding multiple ADCs at the ONUs as compared to that of adding one MZM and two higher-sampling-rate DACs at the OLT. The introduction of ADCs to enable receiver-based post-equalization makes it possible to provide soft information to the decoder. Our current performance analysis is not applicable to soft decoders for the following reasons. First, FEC performance will differ from that of the fixed-initialization LDPC decoding simulations performed. Second, as noted in Section IIIA, the performance metric for soft decoders is GMI rather than pre-FEC BER. Therefore, in the throughput analysis of Section IVC, we consider only transmitter-based pre-equalization and equalization-free options.

By combining the results from simulation of the optical channel with the LDPC code performance, we determine the receiver sensitivity of each modulation format and code rate combination, shown in Fig. 8 for a system employing transmitter-based pre-equalization. Switching from OOK to 3-PAM and from 3-PAM to 4-PAM both require roughly 3 dB of optical power increase, and the receiver sensitivity range is about 10 dB, in agreement with spectral efficiency calculations, but there are penalties from non-ideal pulse shape, signal distortion, ISI, and FEC gap to capacity. Out of the 33 possibilities, considering the tradeoff between receiver complexity and bit rate resolution, we select 14 combinations, circled in Fig. 8, along the outer hull of the bit rate-vs.-receiver sensitivity curves, to use as communication modes. With this subset of modes using all three modulation formats and five different code rates (0.67, 0.75, 0.85, 0.89, 0.92), links with receiver sensitivities ranging from -31 dBm at 20 Gb/s to -22.6 dBm at 54.5 Gb/s are supported.

B. Network Heterogeneity

Each port of an OLT is connected to many ONUs, each with its own channel characteristics. To estimate the effect of this heterogeneity, we create a model for the link variation in an optical network. Fig. 9. Shows the probability density function of the relative optical power loss$p_x(x)$in a representative PON. A deterministic parameter that affects link loss is the length of the distribution fibers that connect the passive optical splitter to each ONU; for ONUs distributed around an OLT, distance is typically Rayleigh distributed [40]. Because the structure of a PON is known, it is possible to specify the maximum length, and we modify the Rayleigh distribution by imposing a finite

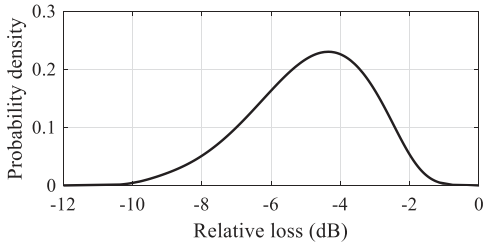

Fig. 9. Example optical power loss probability distribution for a PON including deterministic and random variation.

maximum length. The deterministic component of optical power loss in the PON is then

$$p_{\mathrm{det}}(x) = \frac{-x \exp\left(-x^2/(2s^2)\right)}{s^2\left(1-\exp\left(-L_{\max}^2\alpha^2/(2s^2)\right)\right)},\ x \in [-L_{\max}\alpha, 0], \tag{6}$$

where x is the relative loss in dB, α is the fiber attenuation parameter in dB/km, s is the scaling parameter of the Rayleigh distribution, and $L_{\max}$ is the maximum fiber length.

In addition to the deterministic fiber length distribution, random variables are also present. One example is coupling loss that depends on angular and linear offsets in a connection or splice [41]. Other factors contributing to power variations are temperature shifts and other weather conditions that cause fiber surroundings to change; the effect of these factors is modeled as a log-normal distribution under the assumption that they are largely independent of each other, so the random component of optical power loss in the PON is

$$p_{rnd}(x) = 1/\sqrt{2\pi\sigma^2}\exp\left(-x^2/(2\sigma^2)\right), \tag{7}$$

where σ is the standard deviation of all random factors. By convolving the probability density functions of these three loss sources, we arrive at the final probability distribution

$$p_x(x) = p_{det}(x)^* p_{rnd}(x), \tag{8}$$

where $*$ denotes convolution. Reflecting the distribution from measured data of deployed ONUs, the left tail is slightly longer than the right tail [12].

C. Throughput Increase

To evaluate the performance gain of ACM, we analyze the increase in total network throughput enabled by multiple rates. Using our model for PON statistics, we compare against a reference bit rate of 25 Gb/s in a single-rate system using OOK with only the mother code. The maximum fiber distance is set to 25 km; then, the power is set such that the longest link has a 3-dB optical power margin to accommodate random variation and component aging over the lifetime of the PON. This setup roughly corresponds to a PON with splitting ratio 64 and maximum fiber length 25 km.

We compare fixed-rate transmission to two adaptive-rate transmission schemes. The first, adaptive modulation, uses only the mother code but all three modulation format options. The second, ACM, uses adaptive modulation with three modulation formats as well as adaptive coding with five code rates to utilize the full range of available rates. For all transmission schemes, a margin of 3 dB is maintained for all transmission rates used.

TABLE II
EQUALIZED THROUGHPUT COMPARISON

	Fixed rate	Adaptive modulation		Adaptive coding and modulation	
		No eq.	TX eq.	No eq.	TX eq.
Equalized rate (Gb/s)	25	31.2	36.5	34.3	39.7
	37.5	46.2	48.2	49.3	51.7
	50	50	50	53.9	54.0
Number of modulation formats	1	3		3	
Number of code rates	1	1		5	
Minimum margin (dB)	3	3		3.6	

With rate adaptation, two possible ways to allocate time on the channel are to allocate equal time to each ONU on the TDM channel, or to allocate time for each ONU inversely proportional to its bit rate. Allocating time based on bit rate provides every ONU with the same equalized bit rate. The equalized bit rate corresponds to the maximum rate the system can support with all users achieving the same rate. By enabling ONUs with higher SNR to operate at higher rates, time is freed up for ONUs with lower SNRs, increasing the average rate of all ONUs.

For adaptive modulation with three bit rate options, if each ONU receives equal time on the TDM channel, the maximum time-averaged bit rate is 38.5 Gb/s with pre-equalization, a 54% increase. If instead the amount of time allocated for each ONU is inversely proportional to its bit rate, then every ONU has the same equalized bit rate of 36.5 Gb/s, a 46% increase. ACM increases the maximum averaged bit rate by 66% to 41.4 Gb/s and the equalized bit rate by 59% to 39.7 Gb/s. The equalized bit rates achieved by each transmission setup for the 25 Gb/s reference network configuration with and without transmitter-based pre-equalization are summarized in the first row of Table II. The second and third rows show the throughput increase with ACM if the PON power budget is increased to allow for 3-PAM or 4-PAM fixed-rate transmission, respectively. The use of transmission modes with lower code rates improves the minimum receiver sensitivity and adds extra margin to a network, so the probability that a link fails because the received optical power is too low to support any communication mode decreases. ACM can achieve bit rates greater than 50 Gb/s due to the punctured codes that have higher rate than the mother code, and greater minimum margin due to better receiver sensitivity of shortened codes. Consequently, allowing different code rates in addition to different modulation formats not only increases the overall achievable throughput, it also simultaneously decreases the link failure probability.

Splitting ratio, transmitted power, fiber length, and penalties from component aging over time can all affect the available optical power in a PON. To account for differences among PON structures, Fig. 10a shows the increase in equalized bit rate with received optical power for fixed-rate transmission, adaptive modulation, and ACM with and without transmitter-based pre-equalization. An optical power offset of 0 dB corresponds to

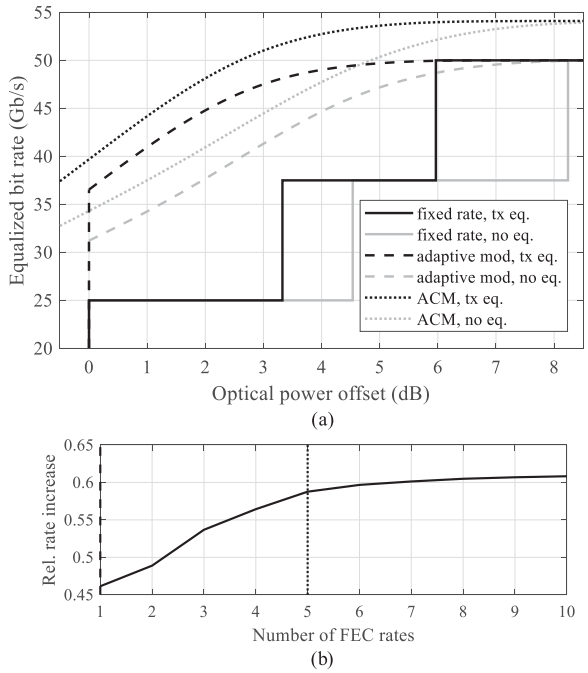

Fig. 10. Throughput increase from ACM. (a) Equalized bit rate as a function of optical power offset to accommodate different power budgets or receiver sensitivities, showing fixed-rate transmission (solid), adaptive modulation using 2-PAM, 3-PAM, and 4-PAM and the mother code (dashed), and ACM with the three modulation orders and five code rates (dotted), without equalization (gray) or with transmitter-based pre-equalization (black). (b) Relative equalized bit rate increase from ACM compared to fixed-rate transmission at 0-dB offset for increasing number of FEC rates. Dotted vertical line indicates the five code rates used to evaluate equalized bit rate for ACM in (a).

3 dB of margin in the worst channel for the 25 Gb/s transmission mode as described initially. An optical power offset corresponds to a uniform increase in available optical power to all ONUs in the PON. The step transitions in the solid fixed-rate line indicate the power offsets at which the modulation order in the fixed-rate system increases and the corresponding equalized bit rates in Table II. For example, 3-PAM at 37.5 Gb/s in a fixed-rate system can be supported at an optical power offset of 3.3 dB, which can be realized by decreasing the splitting ratio to 32 and decreasing the feeder fiber length by 1 km. With ACM and pre-equalization, the same system can support over 50 Gb/s, or keep the equalized bit rate of 37.5 Gb/s while increasing optical power margin by 3.7 dB. In a fixed-rate system, to realize 50 Gb/s with 3 dB of optical power margin, the initial received optical power must be at least -21.3 dBm in all channels, but with adaptive coding and modulation, -24.9 dBm minimum received optical power can realize a bit rate of 50 Gb/s with the same margin. The equalized bit rate starts to plateau as it reaches 54.5 Gb/s, because an increasing fraction of links are limited by the bit rate of the highest transmission mode rate, but a higher-order modulation format such as 8-PAM can be added to extend the transmission mode rate range.

Increasing the resolution of usable bit rates by adding more FEC rates increases the margin and throughput of the system, but there is a diminishing marginal return of adding new FEC rates. Using a single FEC rate corresponds to adaptive modulation only. The shortened code with the lowest rate determines the extra margin added to the system, and the highest punctured code rate determines the maximum rate of the PON. The reported equalized bit rates for ACM use five different FEC rates. Fig. 10b shows that at 0-dB optical power offset, adding five more FEC rates beyond the first five contributes only 1.3% additional bit rate.

V. Discussion and Conclusions

Leveraging information about current channel conditions to adjust bit rate can provide graceful degradation of performance by decreasing bit rates as channel conditions worsen, increasing system robustness. A PON with 25G-class components employing adaptive coding and modulation with 2-, 3-, and 4-ary PAM supports a 10-dB range of received optical powers. Using OOK and a fixed code rate as reference, optical power margin in the worst channels can be increased 1 dB without increasing transmitted optical power, all while increasing the overall bit rate by over 50%. A 50 Gb/s average bit rate is supported on a network with a splitting ratio of 32 and maximum fiber length of 25 km. Adaptive coding and modulation increases the margin in a system, enabling lower failure probabilities and robustness to changes in channel quality over time. As a first analysis, we investigated the two simplified allocation strategies of equal transmission time or equal bit rate for all ONUs, neglecting the effects of time-varying network traffic. To follow up, a more realistic study would additionally consider the performance of ACM using different dynamic bandwidth allocation strategies and with various network demand statistics.

We compared methods to overcome signal distortion from CD and component bandwidth limitations, which becomes critical at 12.5 Gbaud and higher symbol rates. Transmitter-based pre-compensation avoids noise enhancement but requires two DACs and a dual-quadrature MZM. Receiver-based methods can be used with a simple transmitter, whether an electro-absorption modulated laser (EML) or MZM, but require an ADC and DSP at the receiver. To minimize ONU cost and power consumption, it may be best to use transmitter-based downlink compensation. If receiver-based equalization is introduced, then a logical step is to transition to soft-decision decoding for further coding gain. While decoding relying on ADCs to provide soft information requires more complex performance evaluation replacing pre-FEC BER with GMI in channel and coding simulations and leading to different quantitative results, the ACM scheme using multiple modulation formats and a shortened/punctured FEC code, along with the general method for throughput analysis in Section IVC, remains valid.

Another mechanism for rate adaptation is probabilistic shaping. By changing the shaping parameter and thus input probability distribution, different information rates can be realized with the same modulation format and FEC. In coherent systems, probabilistic shaping can provide SNR gain of about 1 dB [19], even using only hard-decision decoding. Probabilistic shaping results in performance that more closely tracks the capacity curve [42] compared to puncturing and shortening that exhibits growing performance penalty as more bits are deleted.

However, a drawback of probabilistic shaping is that probability mappers are complex to implement and can complicate the clock and data recovery process. Most probabilistic shaping studies have focused on coherent systems, but probabilistically shaped PAM in a direct-detection system has been shown to increase achievable information rate by 0.19 bits/symbol and throughput by 11.4% compared to uniformly distributed PAM [43], although the application of probabilistically shaped PAM to rate adaptation in direct-detection systems has yet to be studied.

Our analysis focuses on the downlink, and because we opt to increase network throughput rather than decrease margin, the network structure is unchanged. Therefore, the uplink remains usable and is not affected by rate adaptation on the downlink. However, asymmetric PON protocols reflect that the uplink bit rates are more challenging to increase than the downlink, so applying rate adaptation solely to the downlink will further increase the disparity between uplink and downlink rates. It is possible to apply rate adaptation to the uplink as well, but further analysis is necessary.

ACKNOWLEDGMENT

The authors thank Jose Krause Perin, Liang Du, Cedric Lam, Alex Duque, Vincent Houtsma, Dora van Veen, and Adriaan de Lind van Wijngaarden for helpful discussions.

REFERENCES

[1] *OECD Broadband Statistics Update*, Paris: OECD, 2019.
[2] X. Zhao *et al.*, "Field trial of long-reach TWDM PON for fixed-line wireless convergence," in *Proc. Eur. Conf. Opt. Commun.*, Gothenburg, Sweden, 2017.
[3] Y. Guo *et al.*, "Demonstration of 25 Gbit/s per channel NRZ rransmission with 35 dB power budget using 25G Ge/Si APD for next generation 100G-PON," in *Proc. Opt. Fiber Commun. Conf.*, Washington, D.C., USA, 2017, p. M3H.6.
[4] A. J. Goldsmith and S.-G. Chua, "Adaptive coded modulation for fading channels," *IEEE Trans. Commun.*, vol. 46, no. 5, pp. 595–602, May 1998.
[5] D. A. A. Mello, A. N. Barreto, T. C. de Lima, T. F. Portela, L. Beygi, and J. M. Kahn, "Optical networking with variable-code-rate transceivers," *J. Lightw. Technol.*, vol. 32, no. 2, pp. 257–266, Jan. 2014.
[6] I. B. Djordjevic, "Adaptive modulation and coding for free-space optical channels," *J. Opt. Commun. Netw.*, vol. 2, no. 5, pp. 221–229, May 2010.
[7] G. Kramer, A. Ashikhmin, A. J. van Wijngaarden, and X. Wei, "Spectral efficiency of coded phase-shift keying for fiber-optic communication," *J. Lightw. Technol.*, vol. 21, no. 10, pp. 2438–2445, Oct. 2003.
[8] Ciena, Liquid Spectrum: Transforming static optical networks into dynamic, responsive assets, 2017.
[9] D. Suvakovic *et al.*, "A low-energy rate-adaptive bit-interleaved passive optical network," *IEEE J. Sel. Areas Commun.*, vol. 32, no. 8, pp. 1552–1565, Aug. 2014.
[10] H. Kimura, K. Asaka, H. Nakamura, S. Kimura, and N. Yoshimoto, "First demonstration of energy efficient IM-DD OFDM-PON using dynamic SNR management and adaptive modulation," in *Proc. Eur. Conf. Opt. Commun.*, London, UK, 2013, p. We.4.F.5.
[11] J. Gao, H. Lin, X. Liu, X. Wu, L. Zhou, and S. Yao, "Flexible 2/4-PAM-modulation 25-Gb/s PON for next generation access network," in *Proc. Eur. Conf. Opt. Commun.*, Dusseldorf, Germany, 2016, pp. 941–943.
[12] R. van der Linden, N.-C. Tran, E. Tangdiongga, and A. M. J. Koonen, "Increasing flexibility and capacity in real PON deployments by using 2/4/8-PAM formats," *J. Opt. Commun. Netw.*, vol. 9, no. 1, pp. A1–A8, Jan. 2017.
[13] L. Zhou *et al.*, "Demonstration of software-defined flexible-PON with adaptive data rates between 13.8 Gb/s and 5.2 Gb/s supporting link loss budgets between 15 dB and 35 dB," in *Proc. Eur. Conf. Opt. Commun.*, 2014, p. P.7.24.
[14] J. A. Altabas, D. Izquierdo, J. A. Lazaro, and I. Garces, "1.25–2.5 Gbps cost-effective transceiver based on directly phase modulated VCSEL for flexible access networks," in *Proc. Opt. Fiber Commun. Conf.*, Washington, D.C., 2017, p. Th1K.4.
[15] E. S. Chou and J. M. Kahn, "Adaptive modulation and coding for robust 50G PONs," in *Proc. Int. Conf. Transparent Opt. Netw.*, Angers, France, 2019, p. Th.C1.1.
[16] M. Laubach, S. Yang, R. Hirth, and G. Kramer, "FEC proposal for NGEPON." IEEE P802.3ca 50G-EPON Task Force, Geneva, Switzerland, May 2017. [Online]. Available: http://www.ieee802.org/3/ca/public/meeting_archive/2017/05/laubach_3ca_1_0517.pdf
[17] M. Hagiwara, M. P. C. Fossorier, and H. Imai, "Fixed initialization decoding of LDPC codes over a binary symmetric channel," *IEEE Trans. Inf. Theory*, vol. 58, no. 4, pp. 2321–2329, Apr. 2012.
[18] Physical layer specifications and management parameters for 10 Gb/s passive optical networks, IEEE Standard 802.3av-2009, 2009.
[19] W. Mao and J. M. Kahn, "Lattice codes for amplified direct-detection optical systems," *IEEE Trans. Commun.*, vol. 56, no. 7, pp. 1137–1145, Jul. 2008.
[20] J. Huo *et al.*, "Transmitter and receiver DSP for 112 Gbit/s PAM-4 amplifier-less transmissions using 25G-class EML and APD," *Opt. Exp.*, vol. 26, no. 18, pp. 22673–22686, Sep. 2018.
[21] G. P. Agrawal, "Optical receivers," in *Fiber-Optic Communication Systems*, 4th ed., Hoboken, NJ, USA: John Wiley & Sons Inc., 2010, ch. 4, pp. 128–181.
[22] J. K. Perin, M. Sharif, and J. M. Kahn, "Sensitivity improvement in 100 Gb/s-per-wavelength links using semiconductor optical amplifiers or avalanche photodiodes," *J. Lightw. Technol.*, vol. 34, no. 23, pp. 5542–5553, Oct. 2016.
[23] S. Arimoto, "An algorithm for computing the capacity of arbitrary discrete memoryless channels," *IEEE Trans. Inf. Theory*, vol. IT-18, no. 1, pp. 14–20, Jan. 1972.
[24] G.-H. Gho, L. Klak, and J. M. Kahn, "Rate-adaptive coding for optical fiber transmission systems," *J. Lightw. Technol.*, vol. 29, no. 2, pp. 222–233, Jan. 2011.
[25] Media access control parameters, physical layers, and management parameters for subscriber access networks, IEEE Standard 802.3ah-2004, 2004.
[26] "IEEE P802.3ca 50G-EPON Task Force." [Online]. Available: http://www.ieee802.org/3/ca/
[27] J. Chen and M. P. C. Fossorier, "Near optimum universal belief propagation based decoding of low-density parity check codes," *IEEE Trans. Commun.*, vol. 50, no. 3, pp. 406–414, Mar. 2002
[28] A. Alvarado, E. Agrell, D. Lavery, R. Maher, and P. Bayvel, "Replacing the soft-decision FEC limit paradigm in the design of optical communication systems," *J. Lightw. Technol.*, vol. 33, no. 20, pp. 4338–4352, Oct. 2015.
[29] T. J. Richardson, "Error floors of LDPC codes," in *Proc. Allert. Conf. Commun. Control Comput.*, 2003, pp. 1426–1435.
[30] D. Chang *et al.*, "FPGA verification of a single QC-LDPC code for 100 Gb/s optical systems without error floor down to BER of 10–15," in *Proc. Opt. Fiber Commun. Conf./Natl. Fiber Opt. Eng. Conf.*, Washington, D.C., 2011, p. OTuN2.
[31] N. Jacobsen and R. Soni, "Design of rate-compatible irregular LDPC codes based on edge growth and parity splitting," *IEEE 802.16 Broadband Wirel. Access Work. Gr.*, Nov. 2007.
[32] J. Li and K. R. Narayanan, "Rate-compatible low density parity check codes for capacity-approaching ARQ schemes in packet data communications," in *Proc. Int. Conf. Commun. Internet, Inf. Technol.*, Virgin Islands, USA, 2002, pp. 201–206.
[33] X. Liu, X. Wu, and C. Zhao, "Shortening for erregular QC-LDPC codes," *IEEE Commun. Lett.*, vol. 13, no. 8, pp. 612–614, Aug. 2009.
[34] T. Tian, C. R. Jones, and T. Li, "Construction of rate-compatible LDPC codes utilizing information shortening and parity puncturing," *EURASIP J. Wirel. Commun. Netw.*, vol. 5, pp. 789–795, Dec. 2005.
[35] J. Ha, J. Kim, and S. W. McLaughlin, "Rate-compatible puncturing of low-density parity-check codes," *IEEE Trans. Inf. Theory*, vol. 50, no. 11, pp. 2824–2836, Nov. 2004.
[36] D. Zou and I. B. Djordjevic, "FPGA-based rate-adaptive LDPC-coded modulation for the next generation of optical communication systems," *Opt. Exp.*, vol. 24, no. 18, p. 21159, Sep. 2016.

[37] G. Wang, M. Wu, Y. Sun, and J. R. Cavallaro, "A massively parallel implementation of QC-LDPC decoder on GPU," in *Proc. IEEE Symp. Appl. Specif. Process.*, San Diego, CA, USA, 2011, pp. 82–85.
[38] Y. Xu, B. Liu, L. Gong, B. Rong, and L. Gui, "Improved shortening algorithm for irregular QC-LDPC codes using known bits," *IEEE Trans. Consum. Electron.*, vol. 57, no. 3, pp. 1057–1063, Aug. 2011.
[39] S. Benedetto and G. Bosco, "Channel coding for optical communications," in *Optical Communication Theory and Techniques*, Enrico Forestieri, Ed. New York: Springer, 2005, pp. 63–78.
[40] F. Vacondio *et al.*, "Flexible TDMA access optical networks enabled by burst-mode software defined coherent transponders," in *Proc. Eur. Conf. Exhib. Opt. Commun.*, London, UK, 2013, pp. 393–395, We.1.F.2.
[41] J. M. Nichols, J. V. Michalowicz, and F. Bucholtz, "Distribution of splice loss in single mode optical fiber," *Appl. Opt.*, vol. 57, no. 5, pp. 1140–1150, Feb. 2018.
[42] G. Bocherer, F. Steiner, and P. Schulte, "Bandwidth efficient and rate-matched low-density parity-check coded modulation," *IEEE Trans. Commun.*, vol. 63, no. 12, pp. 4651–4665, Dec. 2015.
[43] T. A. Eriksson, M. Chagnon, F. Buchali, K. Schuh, S. ten Brink, and L. Schmalen, "56 Gbaud probabilistically shaped PAM8 for data center interconnects," in *Proc. Eur. Conf. Opt. Commun.*, Gothenburg, Sweden, 2017.

Elaine S. Chou received the B.S.E. degree from Princeton University, Princeton, NJ, USA, in 2016 and the M.S. degree from Stanford University, Stanford, CA, USA, in 2018, both in electrical engineering, where she is currently working toward the Ph.D. degree in electrical engineering. She interned with Optical Communications Laboratory, Sumitomo Electric Industries Ltd., Yokohama, Japan, in the summer of 2017 and Access Research Lab, Nokia Bell Laboratories, Murray Hill, NJ, USA, in the summer of 2018. Her current research interests include optical fiber communications, modulation and coding techniques, and signal processing.

Joseph M. Kahn (M'90–SM'98–F'00) received the A.B., M.A. and Ph.D. degrees in physics from the University of California, Berkeley, Berkeley, CA, USA, in 1981, 1983, and 1986, respectively. In 1987–1990, he was with AT&T Bell Laboratories. In 1989, he demonstrated the first successful synchronous (i.e., coherent) detection in optical fiber systems, achieving record receiver sensitivity. In 1990–2003, he was on the Electrical Engineering and Computer Sciences faculty, Berkeley. He demonstrated coherent detection of QPSK in 1992. In 1999, along with D.-S. Shiu he authored the first work on shaping and nonequiprobable signaling for optical communications. In the 1990s and early 2000s, he and collaborators performed seminal work on indoor and outdoor free-space optical communications and multi-input multi-output wireless communications. In 2000, he and K.-P. Ho founded StrataLight Communications, whose 40 Gb/s-per-wavelength long-haul fiber transmission systems were deployed widely by AT&T, Deutsche Telekom, and other carriers. In 2002, Ho and Kahn patented the first electronic compensation of fiber Kerr nonlinearity. StrataLight was acquired by Opnext in 2009. In 2003, he became a Professor of Electrical Engineering in the E. L. Ginzton Laboratory, Stanford University, Stanford, CA, USA. In 2008, along with E. Ip he (and G. Li independently) invented simplified digital backpropagation for compensating fiber Kerr nonlinearity and dispersion. Since 2004, he and collaborators have studied propagation, modal statistics, spatial multiplexing, and imaging in multi-mode fibers, explaining the existence of principal modes in 2005, deriving the statistics of coupled modal group delays and gains in 2011, and deriving resolution limits for imaging in 2013. His current research addresses optical comb generators, coherent data center links, rate-adaptive access networks, fiber Kerr nonlinearity mitigation, ultra-long-haul submarine links, and optimal free-space transmission through atmospheric turbulence. He was the recipient of the National Science Foundation Presidential Young Investigator Award in 1991.